Supporting Information

Synthesis and Properties of a Compositional Series of MIL-53(Al) Metal–Organic Framework Crystal-Glass Composites

Christopher W. Ashling[1], Duncan N. Johnstone[1], Remo N. Widmer[2], Jingwei Hou[1], Sean M. Collins[1], Adam F. Sapnik[1], Alice M. Bumstead[1], Paul A. Midgley[1], Philip A. Chater[3], David A. Keen[4], Thomas D. Bennett[1*]

[1]. Department of Materials Science and Metallurgy, University of Cambridge, Cambridge, CB3 0FS, U.K.

[2]. Department of Earth Sciences, University of Cambridge, Downing Street, Cambridge, CB2 3EQ, U.K.

[3]. Diamond Light Source Ltd., Diamond House, Harwell Campus, Didcot, Oxfordshire, OX11 0DE, U.K.

[4]. ISIS Facility, Rutherford Appleton Laboratory, Harwell Campus, Didcot, Oxfordshire, OX11 0QX, U.K.

SCANNING ELECTRON MICROSCOPY IMAGES

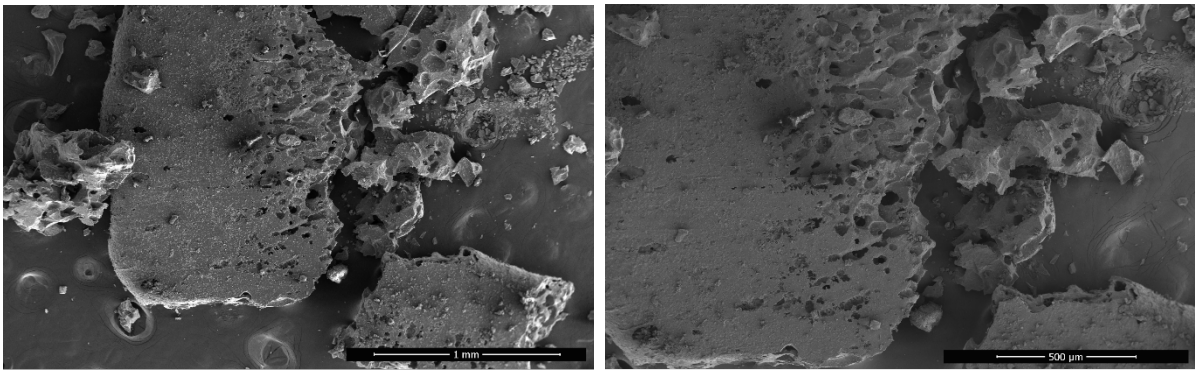

Supplementary Figure 1. SEM images of $(MIL\text{-}53)_{0.3}(a_gZIF\text{-}62)_{0.7}$.

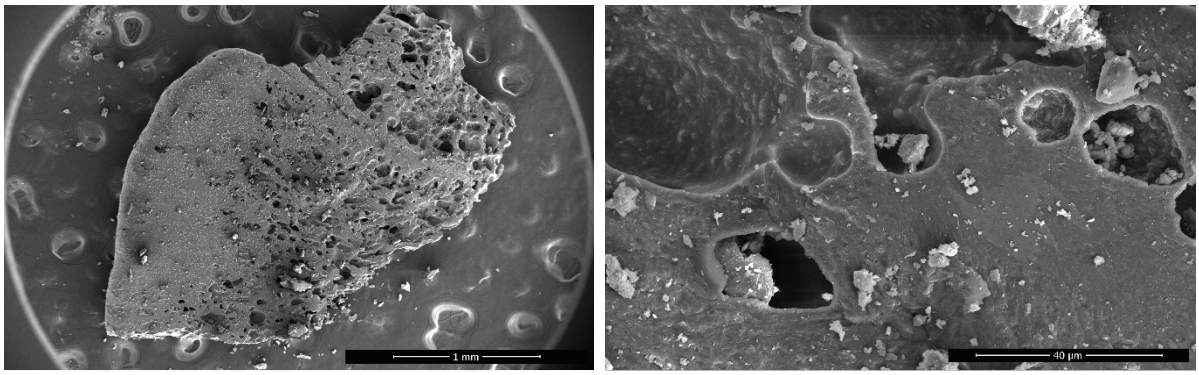

Supplementary Figure 2. SEM images of $(MIL\text{-}53)_{0.4}(a_gZIF\text{-}62)_{0.6}$.

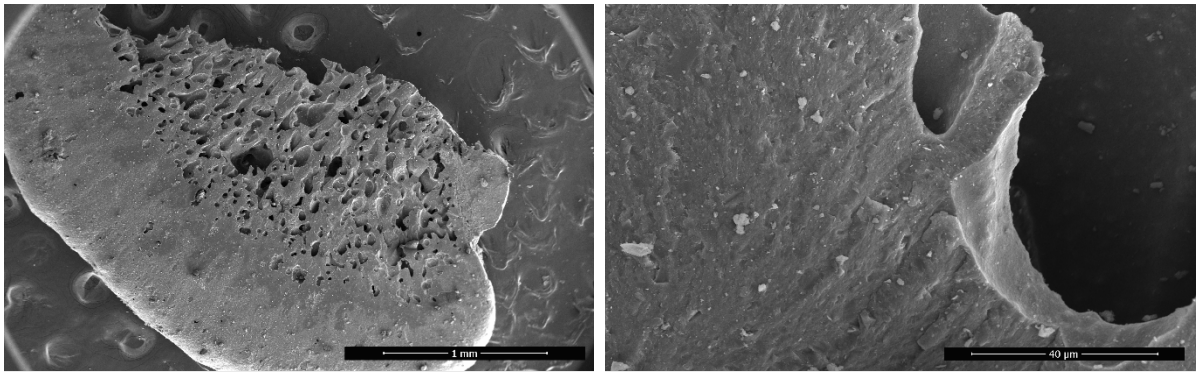

Supplementary Figure 3. SEM images of $(MIL\text{-}53)_{0.5}(a_gZIF\text{-}62)_{0.5}$.

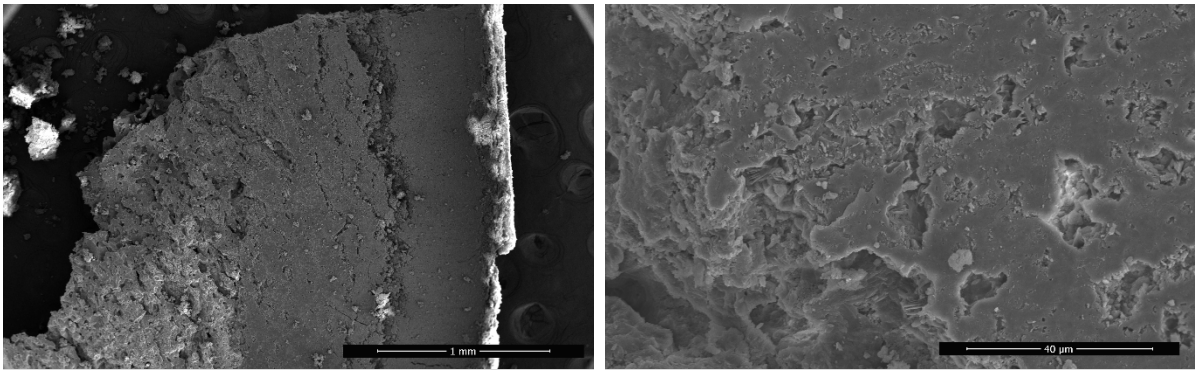

Supplementary Figure 4. SEM images of $(MIL\text{-}53)_{0.7}(a_gZIF\text{-}62)_{0.3}$.

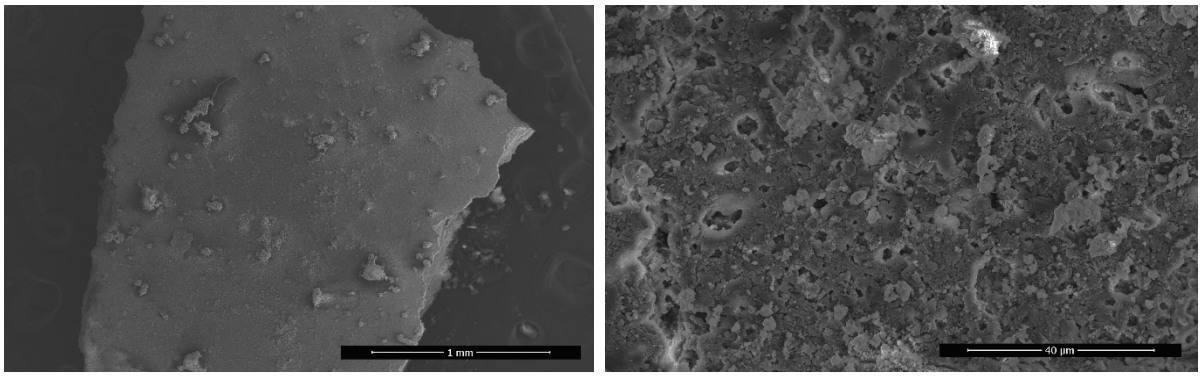

Supplementary Figure 5. SEM images of $(MIL\text{-}53)_{0.8}(a_gZIF\text{-}62)_{0.2}$.

POWDER X-RAY DIFFRACTION

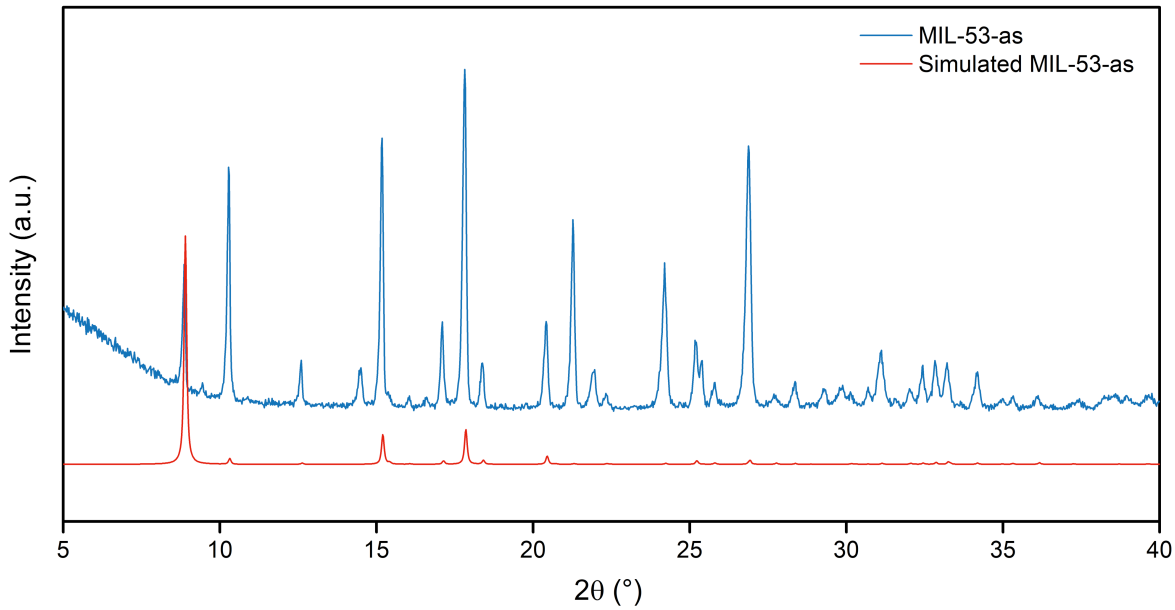

Supplementary Figure 6. MIL-53-as synthesised and simulated patterns.

X-RAY SYNCHROTRON TOTAL SCATTERING DATA

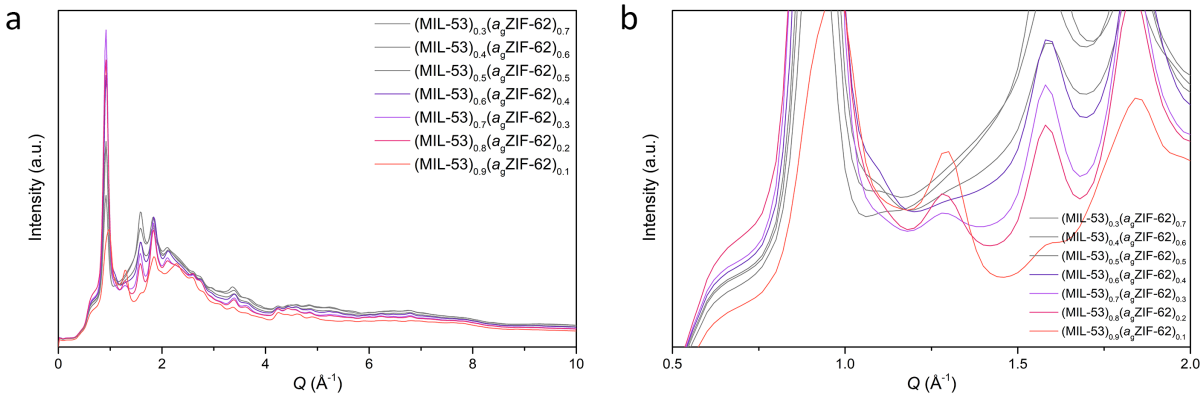

Supplementary Figure 7. X-ray synchrotron total scattering data for all samples of $(MIL\text{-}53)_x(a_gZIF\text{-}62)_{1-x}$ at Q ranges of; **a)** 0-10 Å^{-1}, and **b)** 0.5-2.0 Å^{-1}.

RIETVELD REFINEMENTS OF TOTAL SCATTERING DATA

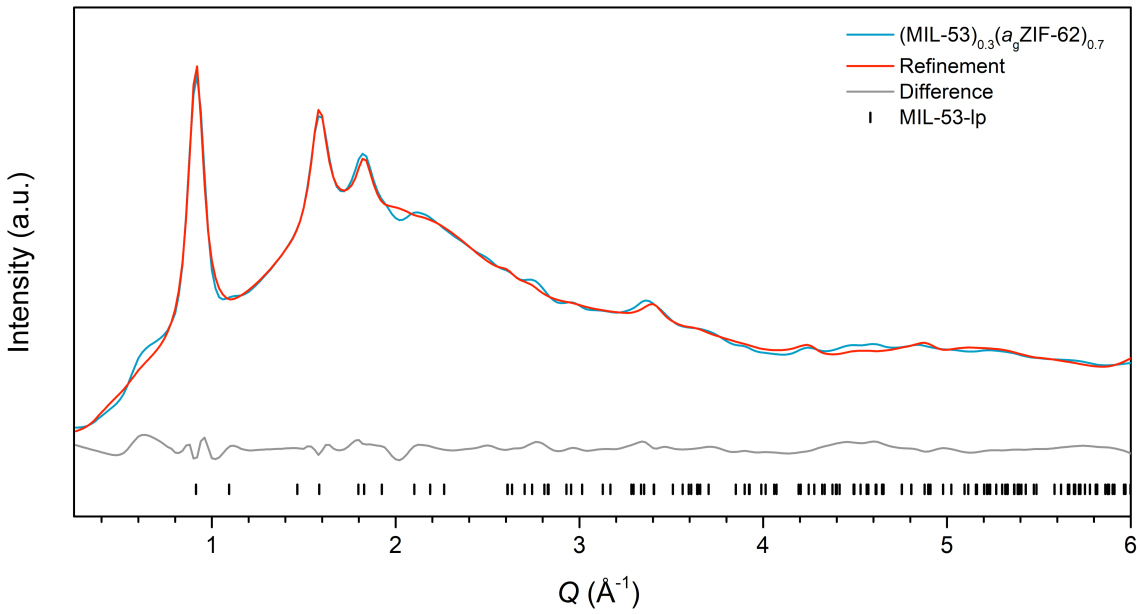

Supplementary Figure 8. X-ray synchrotron total scattering data, Rietveld refinement, difference, and hkl tick marks for $(MIL\text{-}62)_{0.3}(a_gZIF\text{-}62)_{0.7}$.

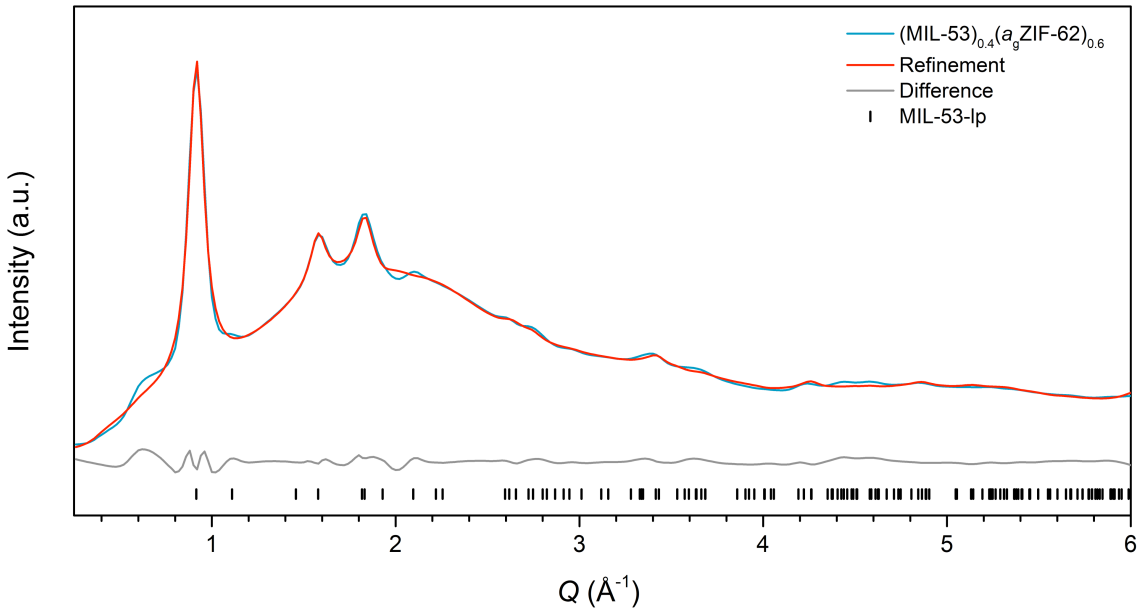

Supplementary Figure 9. X-ray synchrotron total scattering data, Rietveld refinement, difference, and hkl tick marks for $(MIL\text{-}62)_{0.4}(a_gZIF\text{-}62)_{0.6}$.

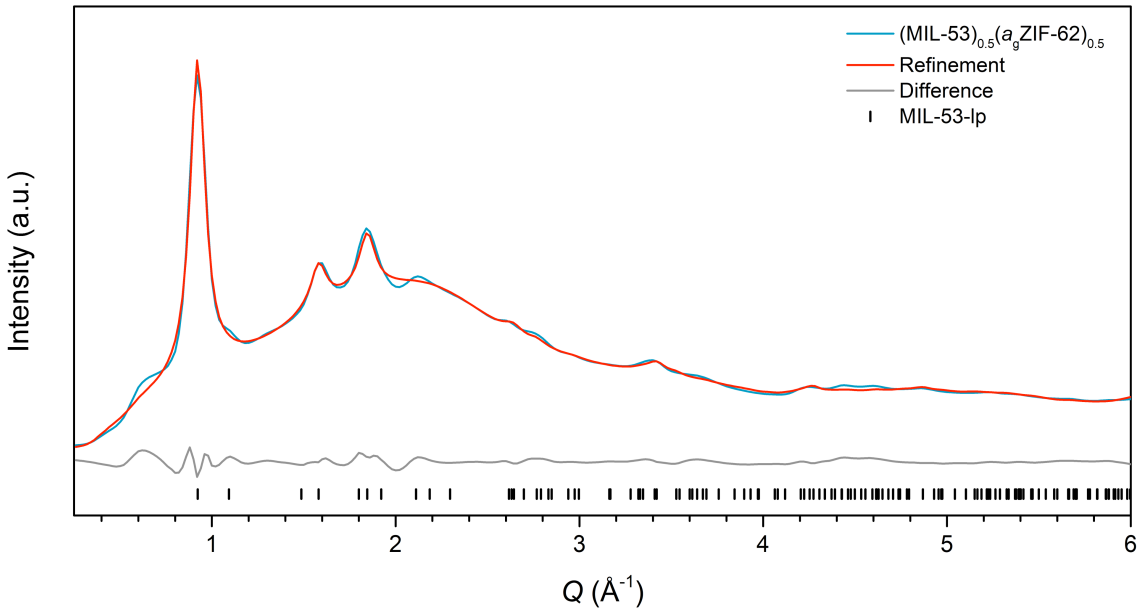

Supplementary Figure 10. X-ray synchrotron total scattering data, Rietveld refinement, difference, and hkl tick marks for $(MIL\text{-}62)_{0.5}(a_gZIF\text{-}62)_{0.5}$.

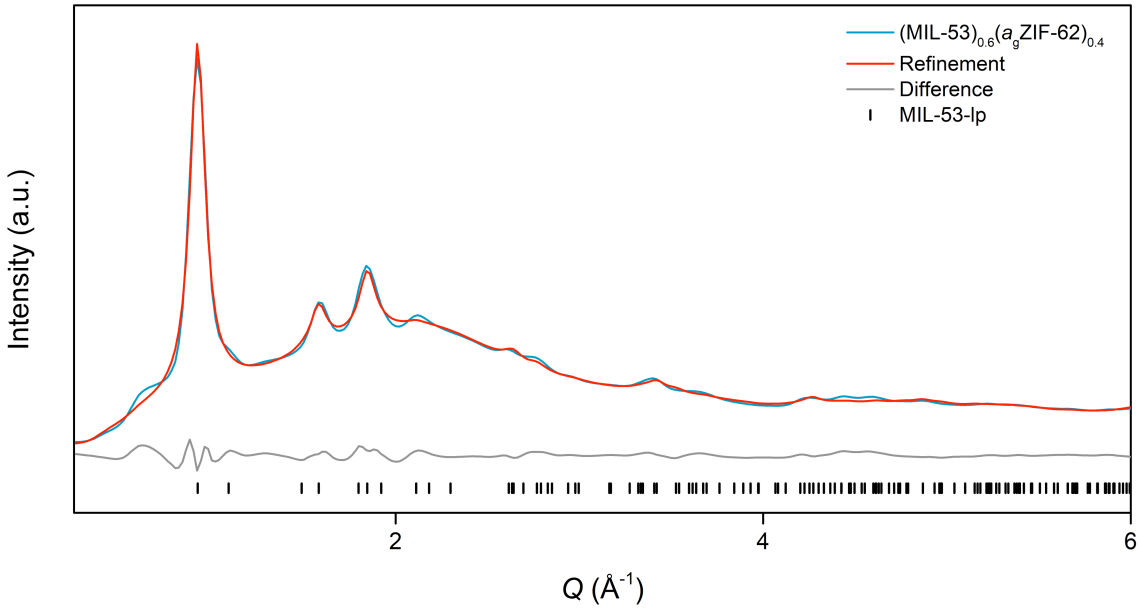

Supplementary Figure 11. X-ray synchrotron total scattering data, Rietveld refinement, difference, and hkl tick marks for $(MIL\text{-}62)_{0.6}(a_gZIF\text{-}62)_{0.4}$.

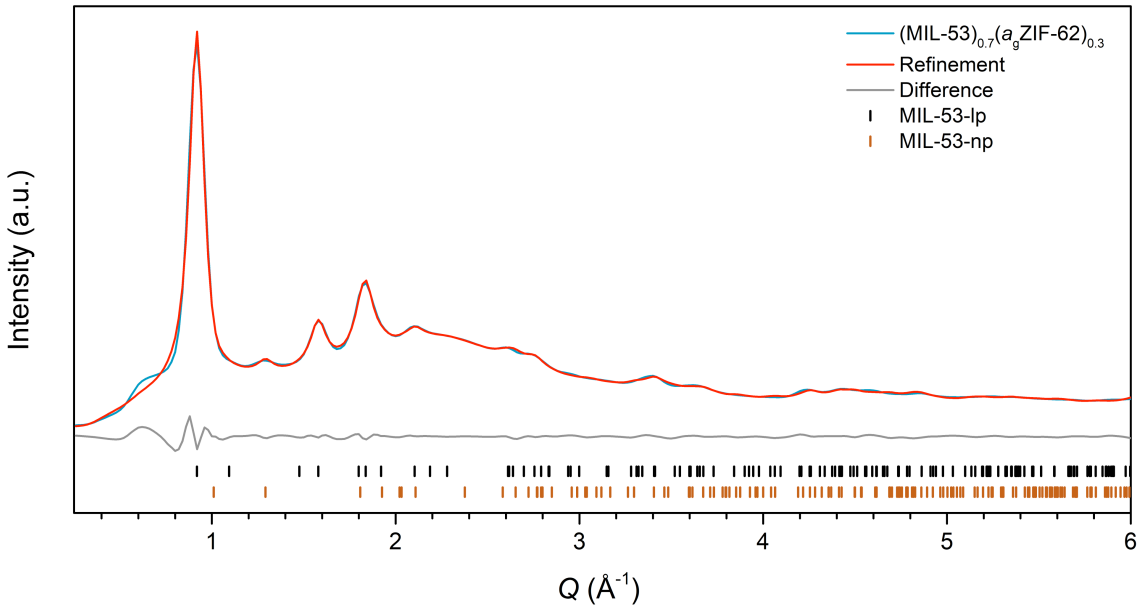

Supplementary Figure 12. X-ray synchrotron total scattering data, Rietveld refinement, difference, and hkl tick marks for $(MIL\text{-}62)_{0.7}(a_gZIF\text{-}62)_{0.3}$.

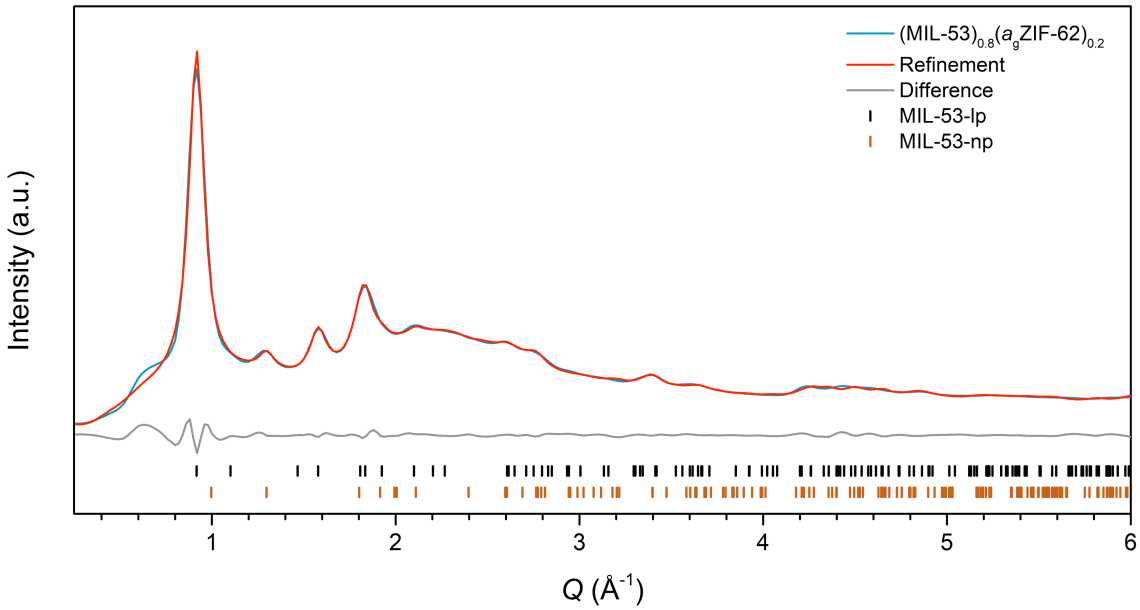

Supplementary Figure 13. X-ray synchrotron total scattering data, Rietveld refinement, difference, and hkl tick marks for $(MIL\text{-}62)_{0.8}(a_gZIF\text{-}62)_{0.2}$.

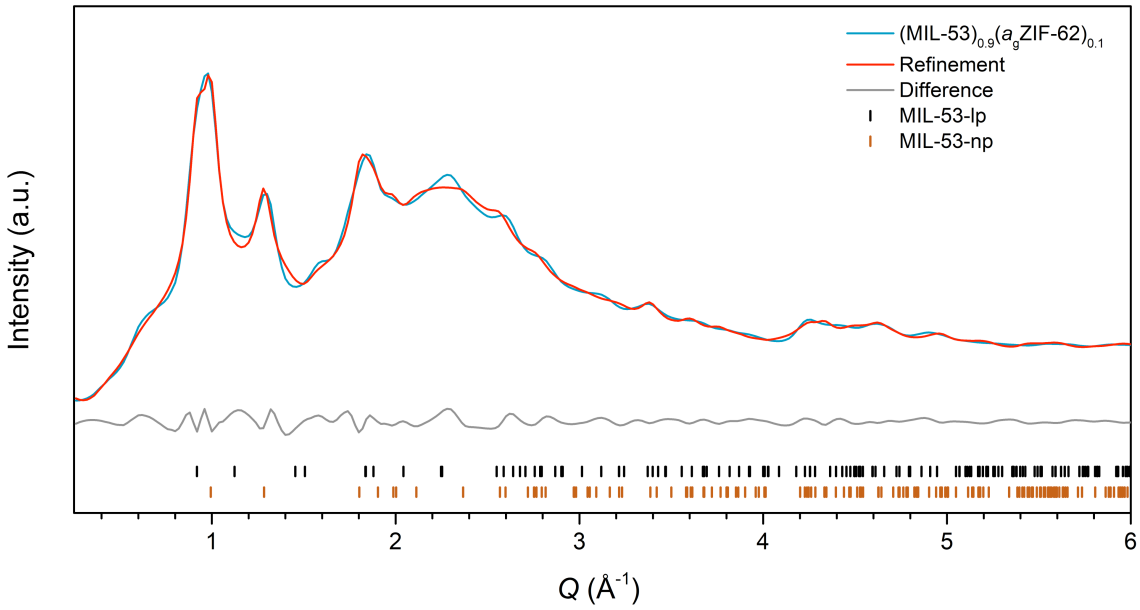

Supplementary Figure 14. X-ray synchrotron total scattering data, Rietveld refinement, difference, and hkl tick marks for $(MIL\text{-}62)_{0.9}(a_gZIF\text{-}62)_{0.1}$.

SCANNING TRANSMISSION ELECTRON MICROSCOPY

Scanning transmission electron microscopy of MOF-CGC particles showing, **(a)** Compositional maps of Al and Zn metal centres from STEM-EDS mapping, **(b)** Annular dark-field images and, **(c)** Crystallinity maps showing the number of Bragg peaks as a function of probe position in SED data for samples of $(MIL\text{-}53)_{0.6}(a_gZIF\text{-}62)_{0.4}$, $(MIL\text{-}53)_{0.7}(a_gZIF\text{-}62)_{0.3}$, and $(MIL\text{-}53)_{0.9}(a_gZIF\text{-}62)_{0.1}$. The color intensity scale for the crystallinity maps showing the number of Bragg scattering peaks identified at each probe position in the scanned field of view is presented for reference. Two different particles shown in top and bottom images. All images are on the same scale.

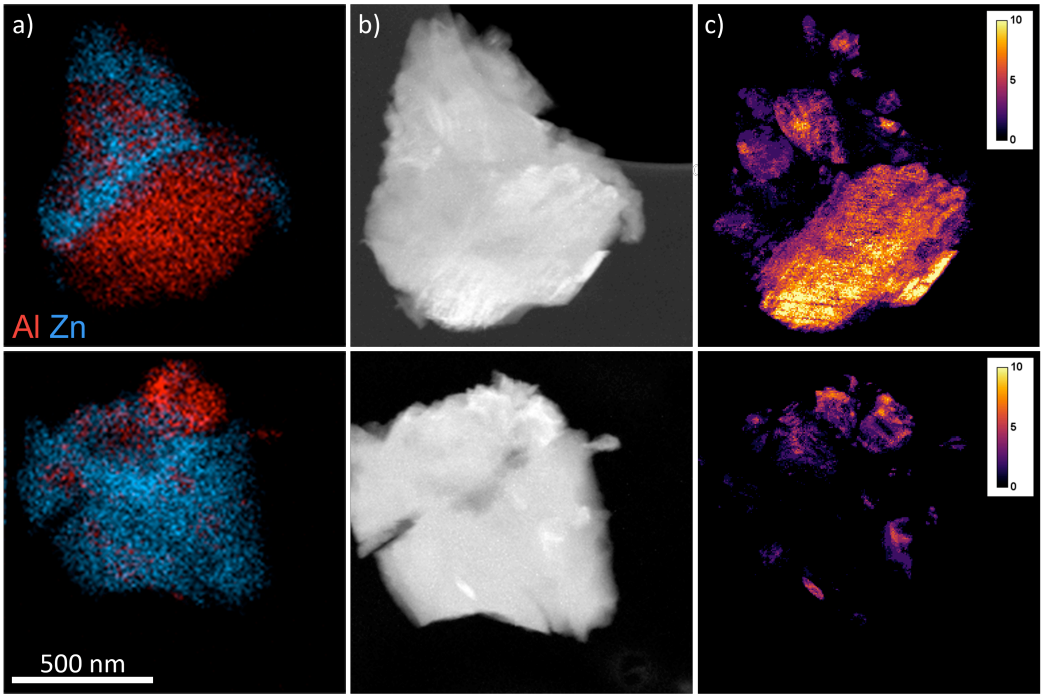

Supplementary Figure 15. Two samples of $(MIL\text{-}53)_{0.6}(a_gZIF\text{-}62)_{0.4}$.

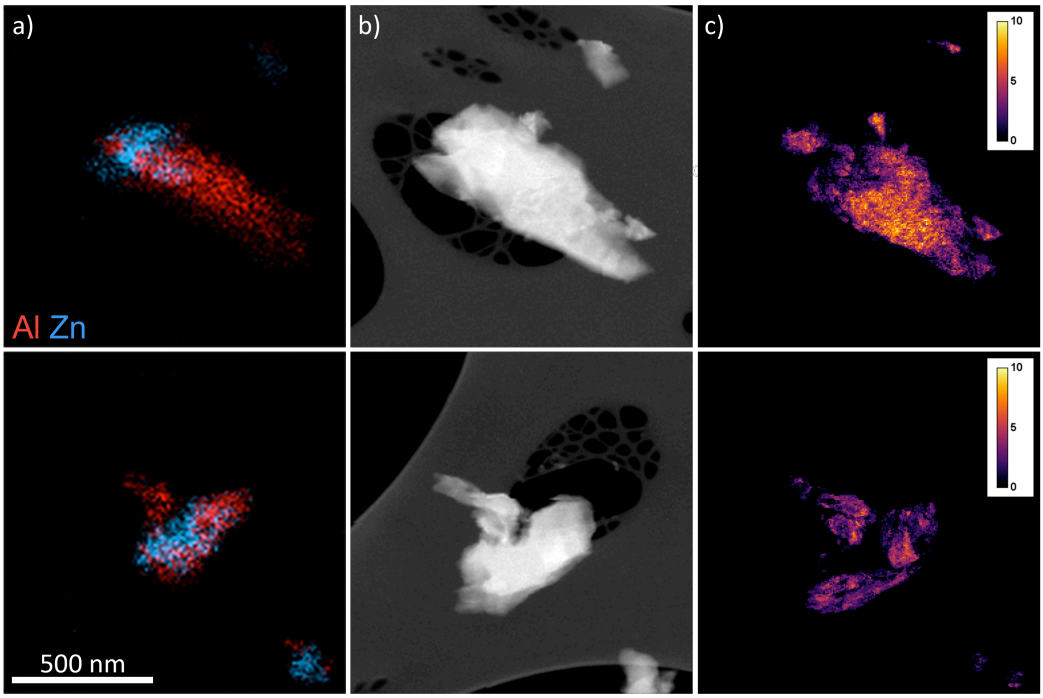

Supplementary Figure 16. Two samples of $(MIL\text{-}53)_{0.7}(a_gZIF\text{-}62)_{0.3}$.

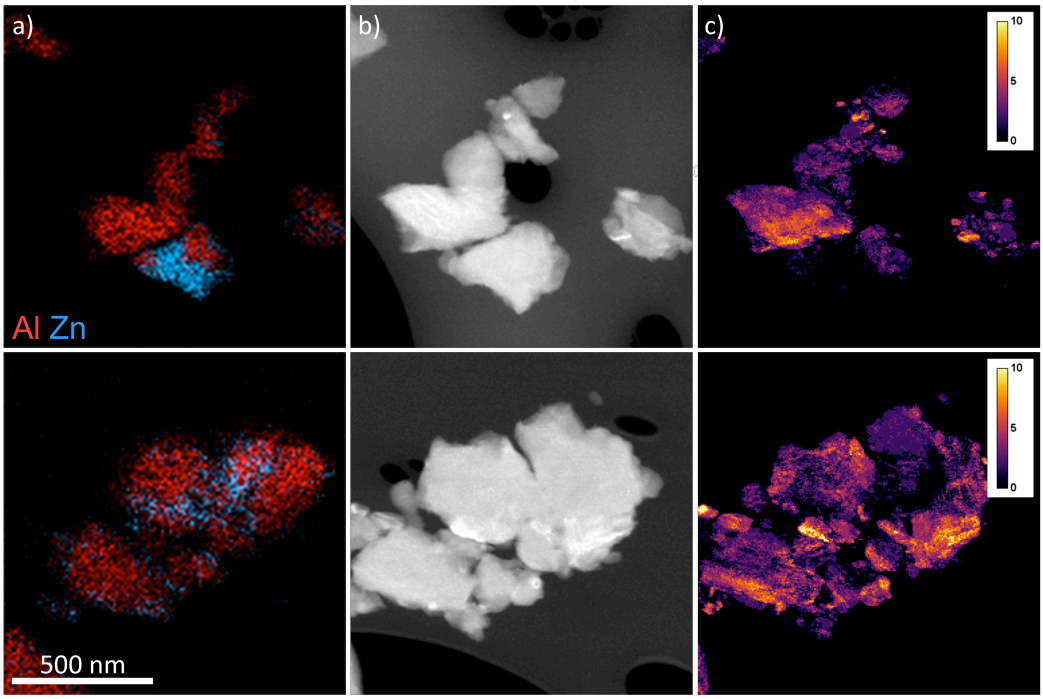

Supplementary Figure 17. Two samples of $(MIL\text{-}53)_{0.9}(a_gZIF\text{-}62)_{0.1}$.

PAIR DISTRIBUTION FUNCTION ANALYSIS

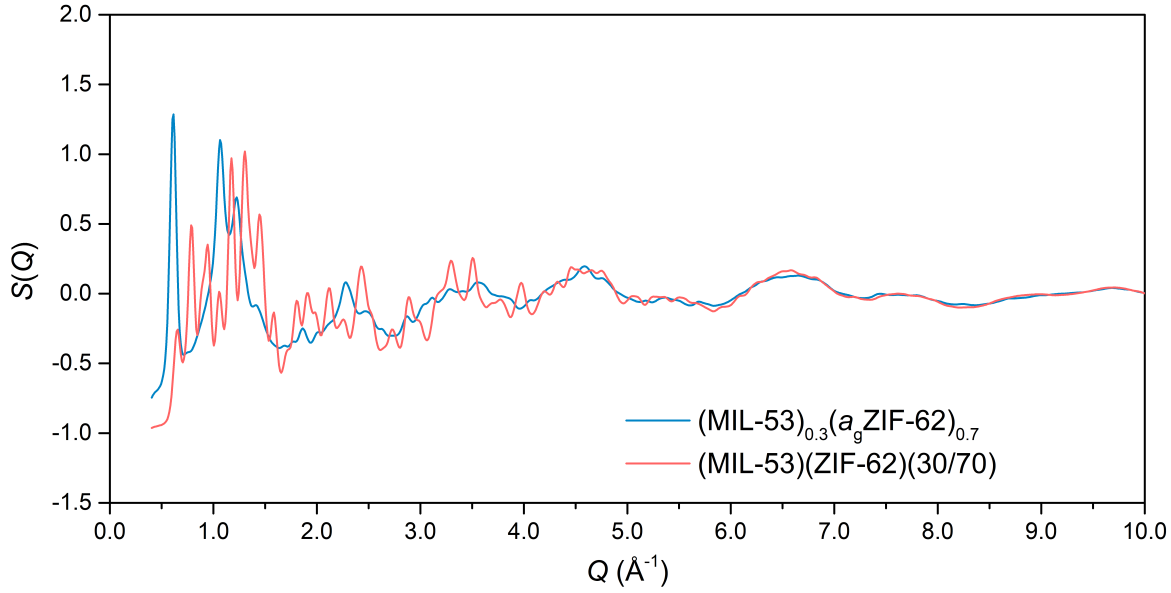

Supplementary Figure 18. Total scattering structure factor, $S(Q)$, data of the crystalline mixture and corresponding MOF-CGC of (MIL-53)(ZIF-62)(30/70) and (MIL-53)$_{0.3}$(a_gZIF-62)$_{0.7}$ respectively.

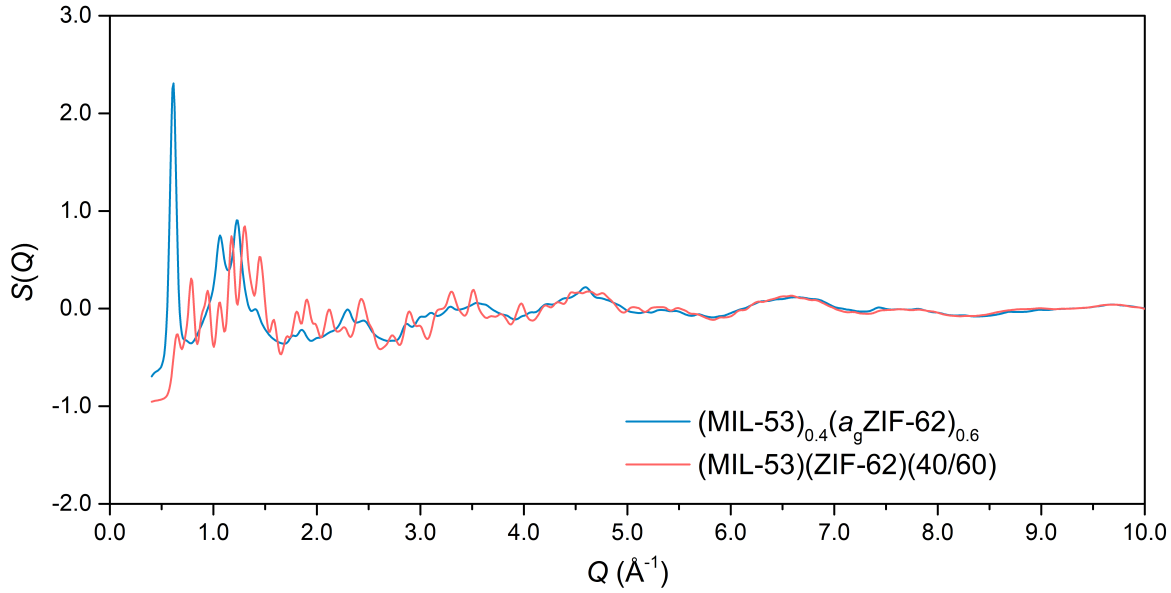

Supplementary Figure 19. Total scattering structure factor, $S(Q)$, data of the crystalline mixture and corresponding MOF-CGC of (MIL-53)(ZIF-62)(40/60) and (MIL-53)$_{0.4}$(a_gZIF-62)$_{0.6}$ respectively.

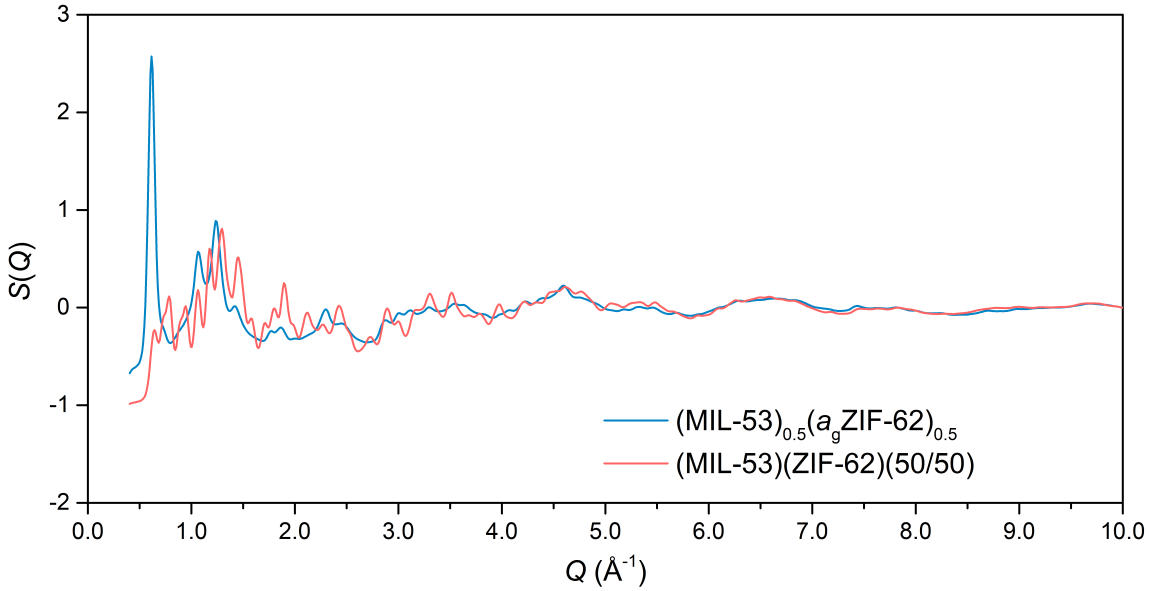

Supplementary Figure 20. Total scattering structure factor, $S(Q)$, data of the crystalline mixture and corresponding MOF-CGC of (MIL-53)(ZIF-62)(50/50) and $(MIL\text{-}53)_{0.5}(a_gZIF\text{-}62)_{0.5}$ respectively.

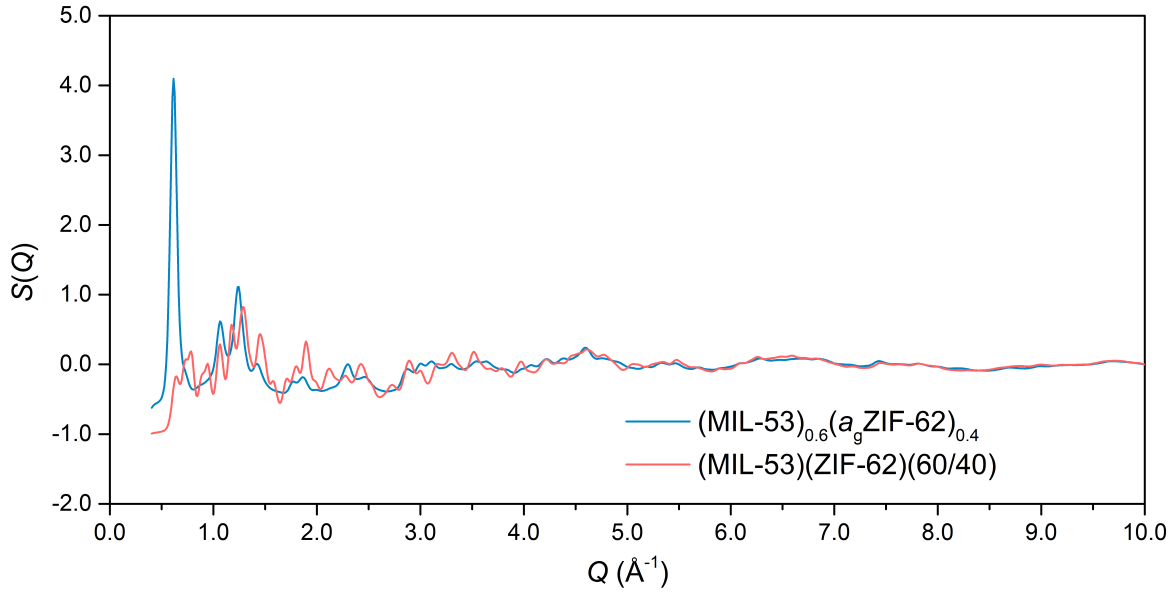

Supplementary Figure 21. Total scattering structure factor, $S(Q)$, data of the crystalline mixture and corresponding MOF-CGC of (MIL-53)(ZIF-62)(60/40) and $(MIL\text{-}53)_{0.6}(a_gZIF\text{-}62)_{0.4}$ respectively.

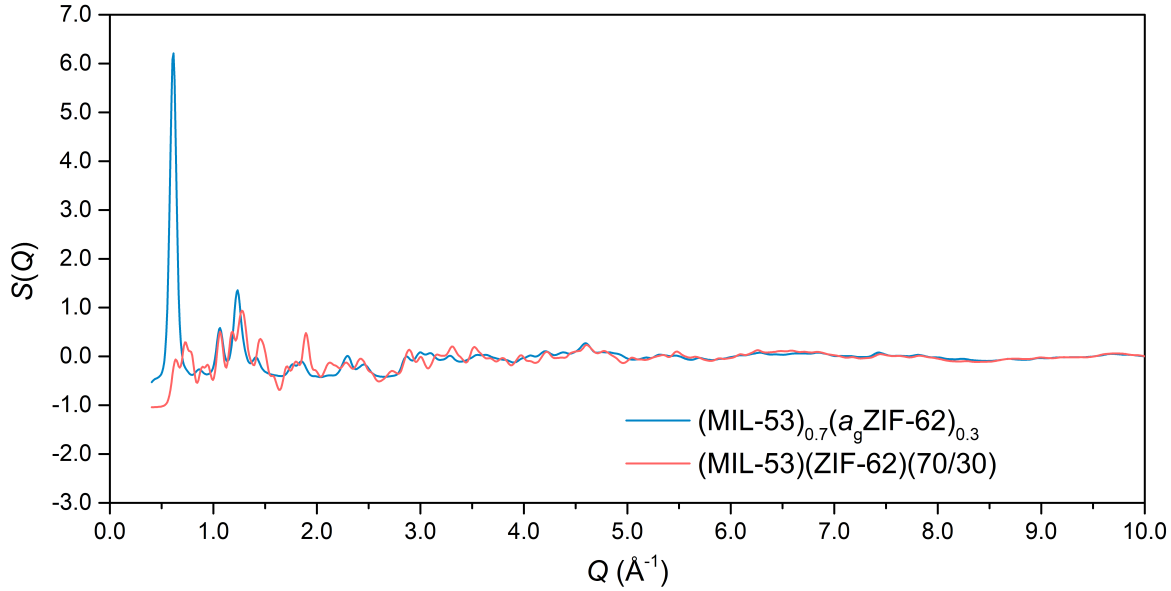

Supplementary Figure 22. Total scattering structure factor, $S(Q)$, data of the crystalline mixture and corresponding MOF-CGC of (MIL-53)(ZIF-62)(70/30) and $(MIL\text{-}53)_{0.7}(a_gZIF\text{-}62)_{0.3}$ respectively.

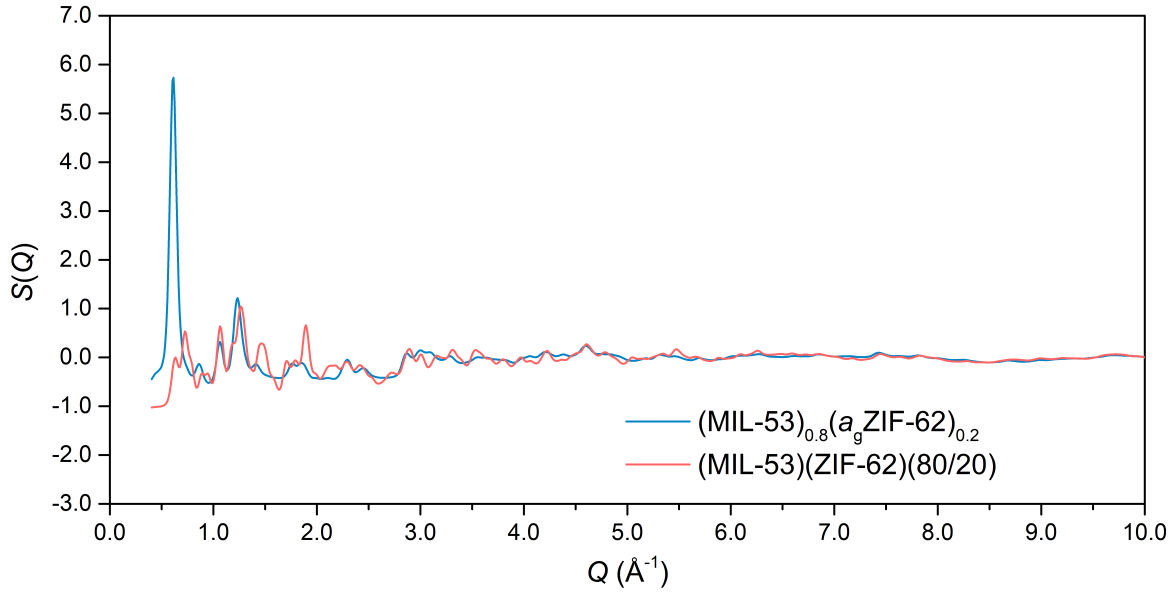

Supplementary Figure 23. Total scattering structure factor, $S(Q)$, data of the crystalline mixture and corresponding MOF-CGC of (MIL-53)(ZIF-62)(80/20) and $(MIL\text{-}53)_{0.8}(a_gZIF\text{-}62)_{0.2}$ respectively.

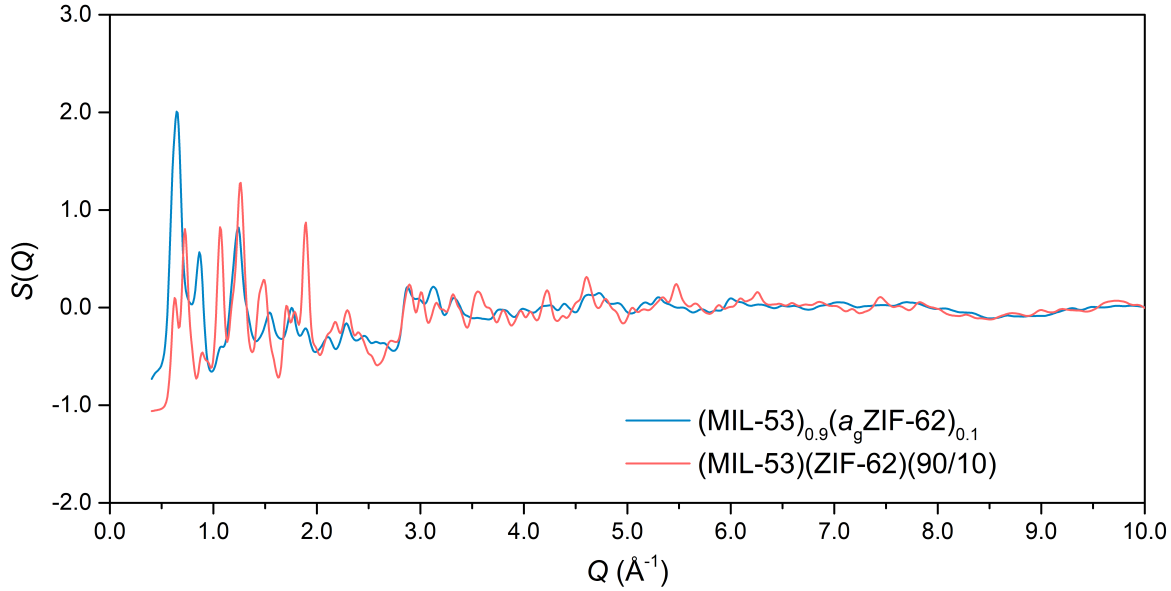

Supplementary Figure 24. Total scattering structure factor, $S(Q)$, data of the crystalline mixture and corresponding MOF-CGC of (MIL-53)(ZIF-62)(90/10) and $(MIL\text{-}53)_{0.9}(a_gZIF\text{-}62)_{0.1}$ respectively.

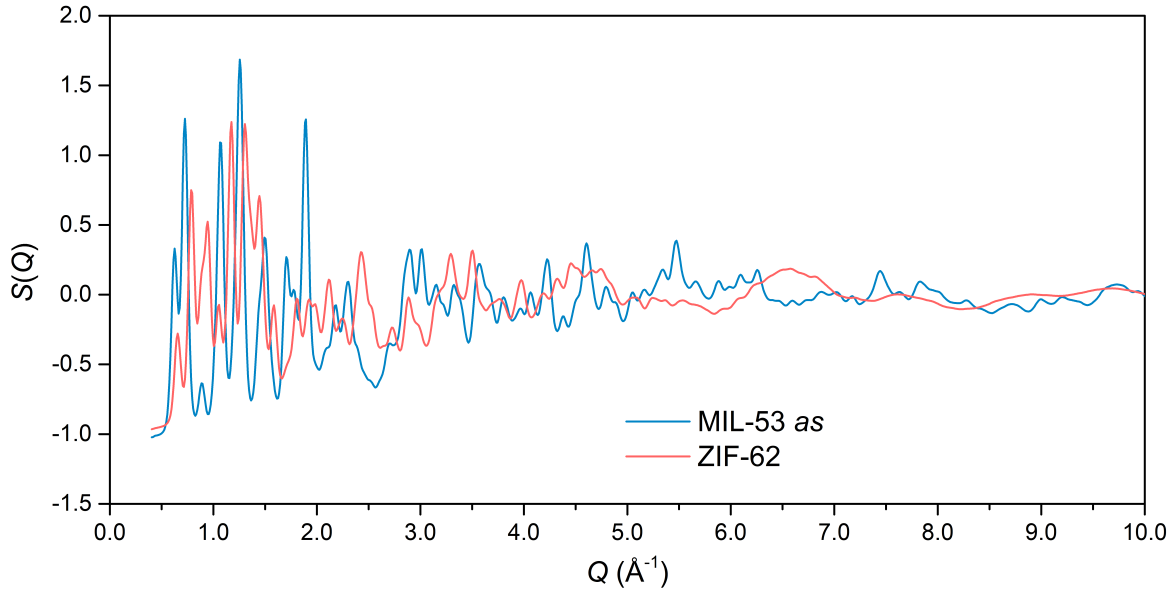

Supplementary Figure 25. Total scattering structure factor, $S(Q)$, data of MIL-53-as and ZIF-62.

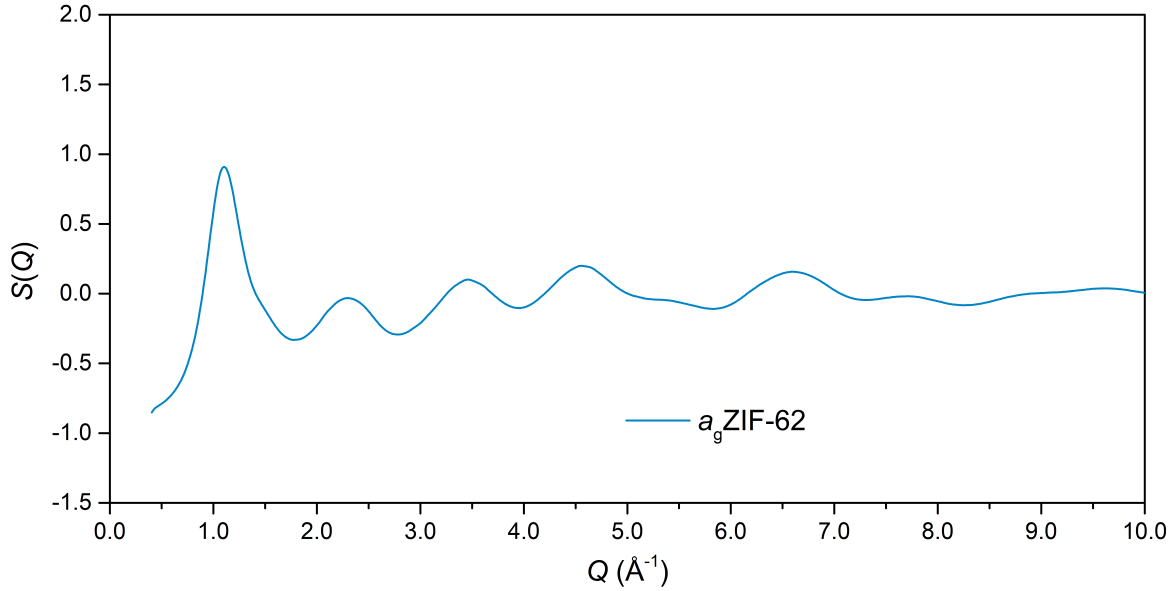

Supplementary Figure 26. Total scattering structure factor, $S(Q)$, data of a_gZIF-62.

PREDICTED PDF PATTERNS

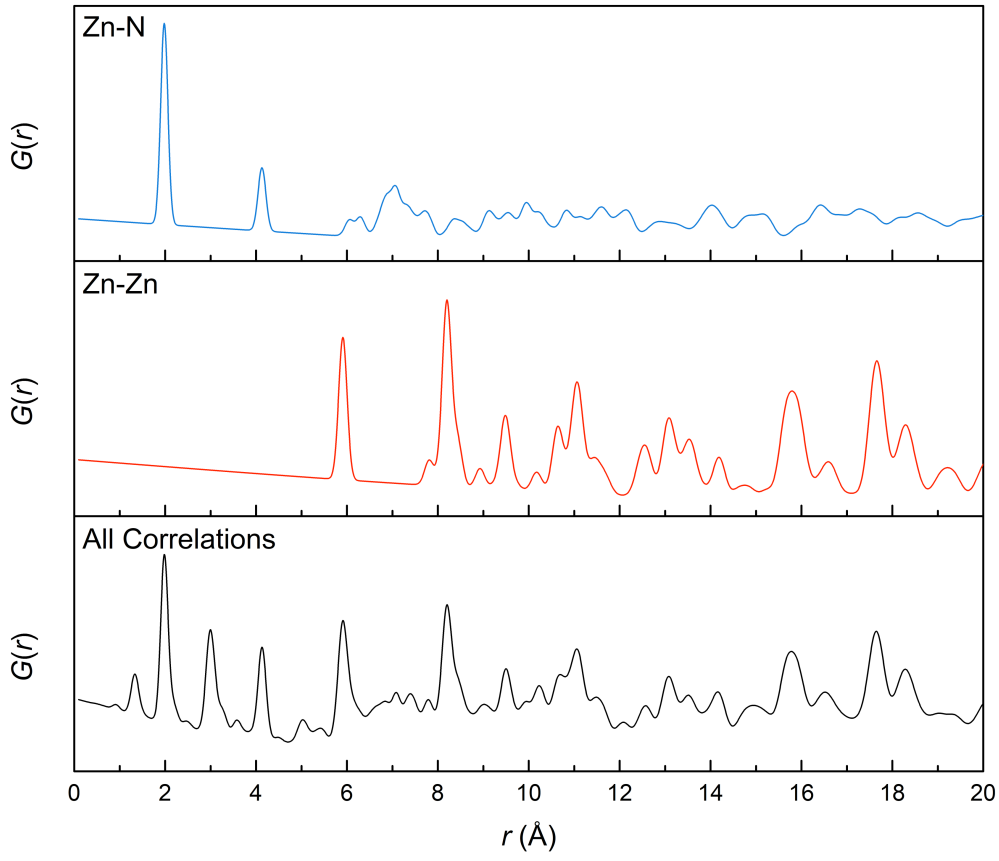

Supplementary Figure 27. Simulated $G(r)$ data of ZIF-62.

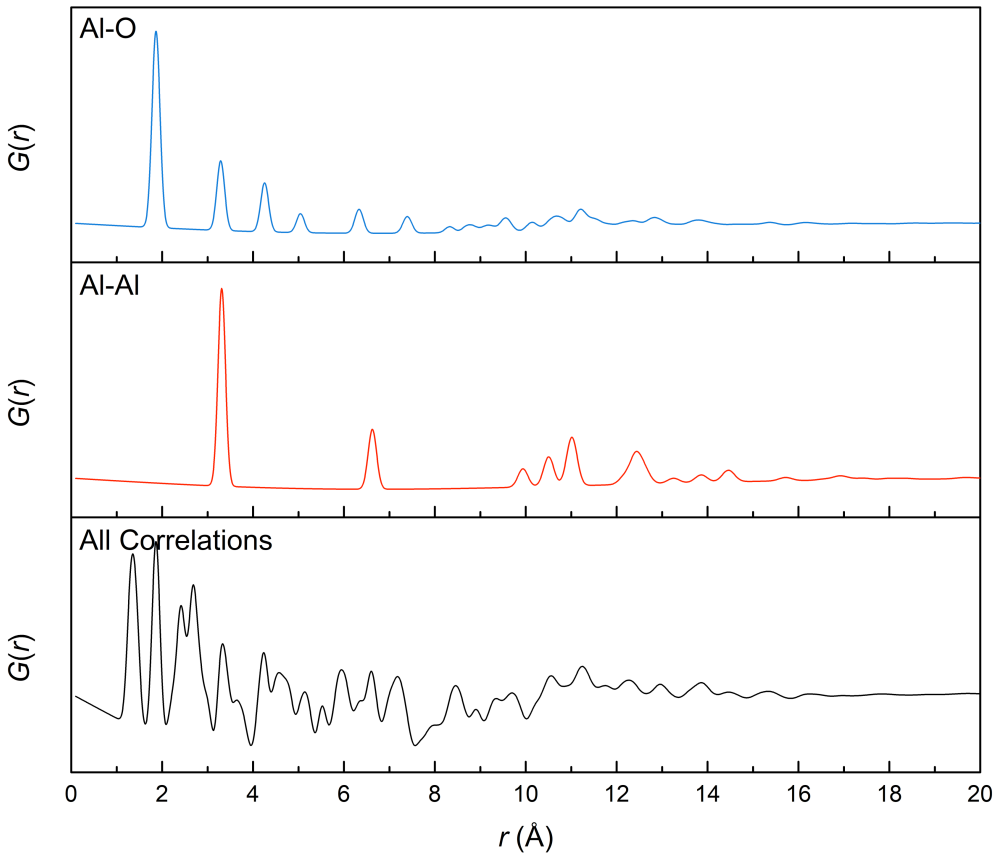

Supplementary Figure 28. Simulated $G(r)$ data of MIL-53-as.

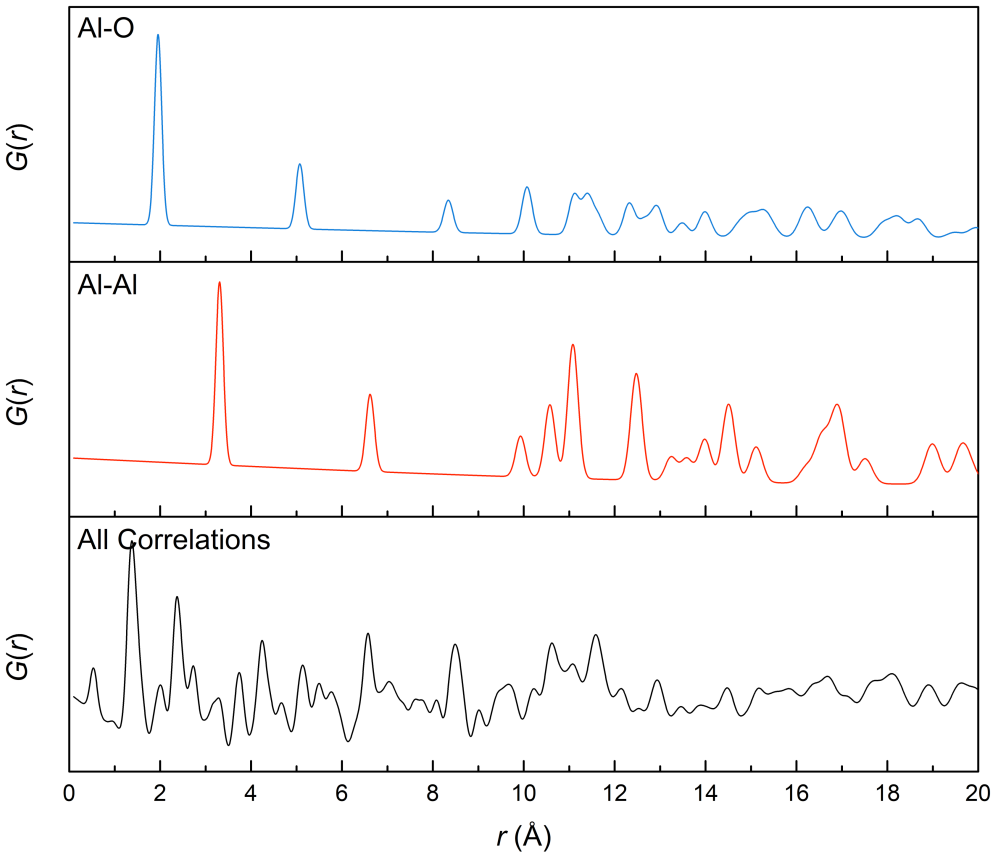

Supplementary Figure 29. Simulated $G(r)$ data of MIL-53-lp.

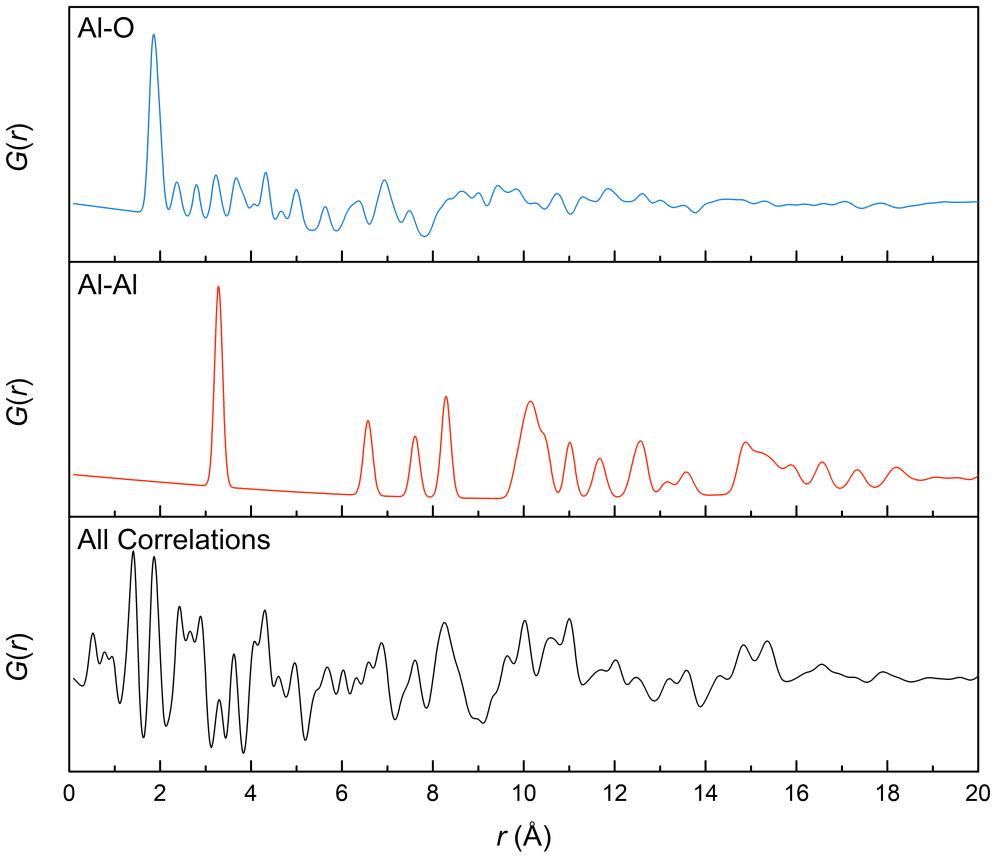

Supplementary Figure 30. Simulated $G(r)$ data of MIL-53-np.

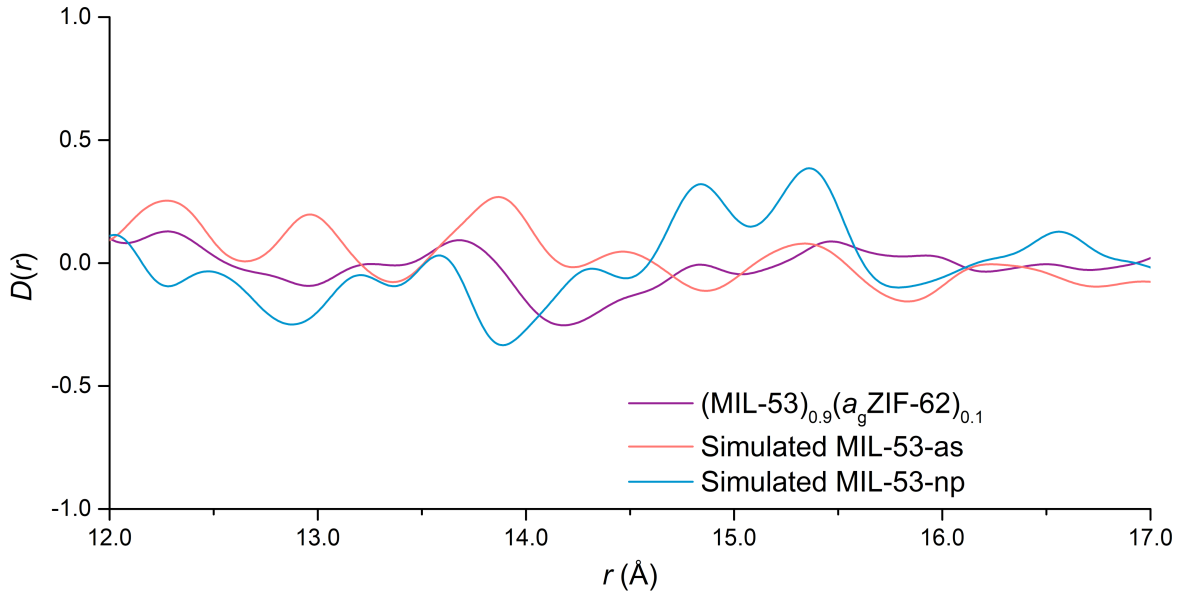

Supplementary Figure 31. Comparison of $(MIL\text{-}53)_{0.9}(a_gZIF\text{-}62)_{0.1}$ with PDFs of MIL-53-as and MIL-53-np simulated using their respective crystalline structures in PDFGUI.

GAS SORPTION

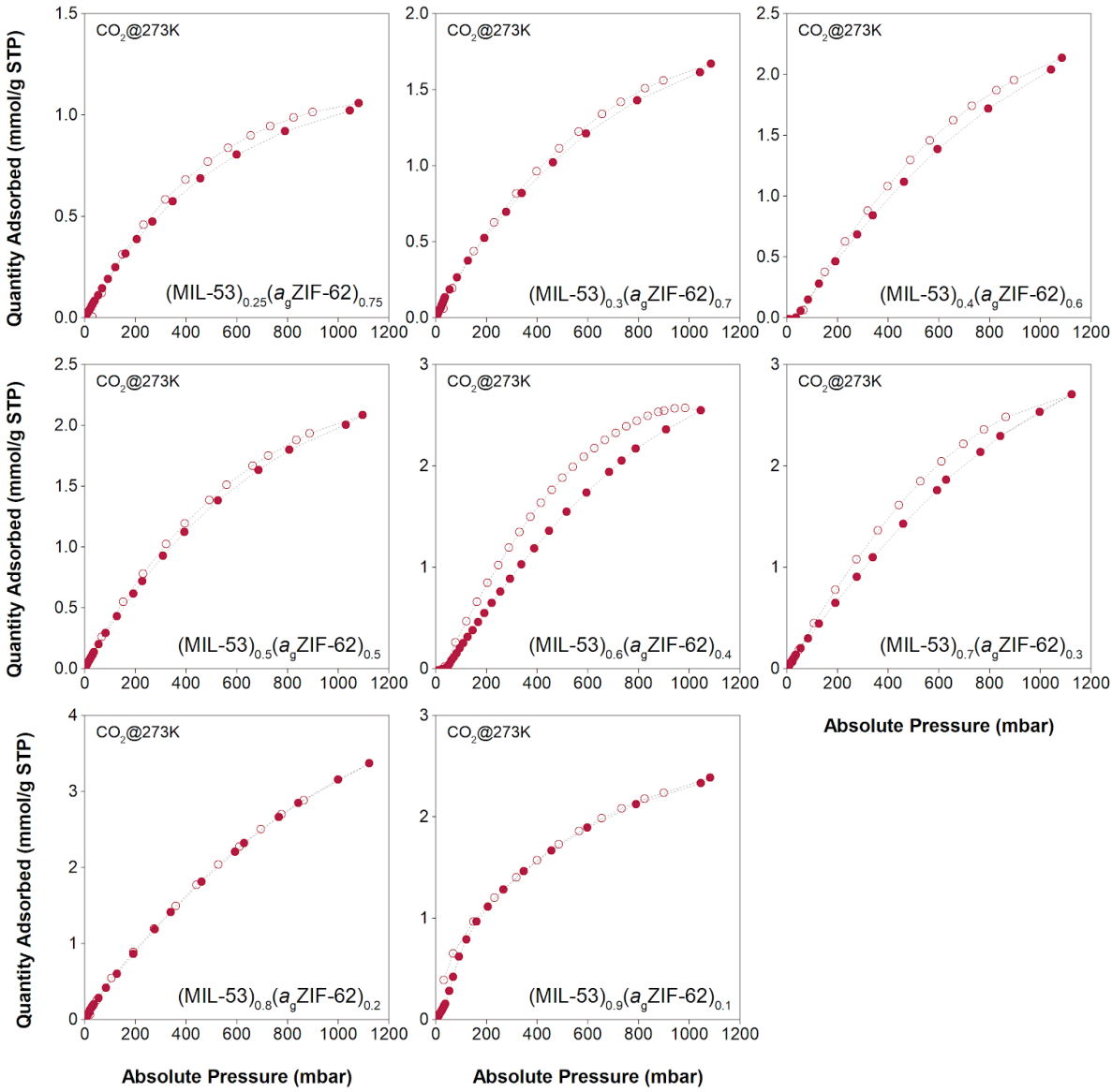

Supplementary Figure 32. CO_2 gas adsorption (solid points) and desorption (open points) isotherms of $(MIL\text{-}53)_x(a_gZIF\text{-}62)_{1-x}$ series recorded at 273 K.

IR ANALYSIS

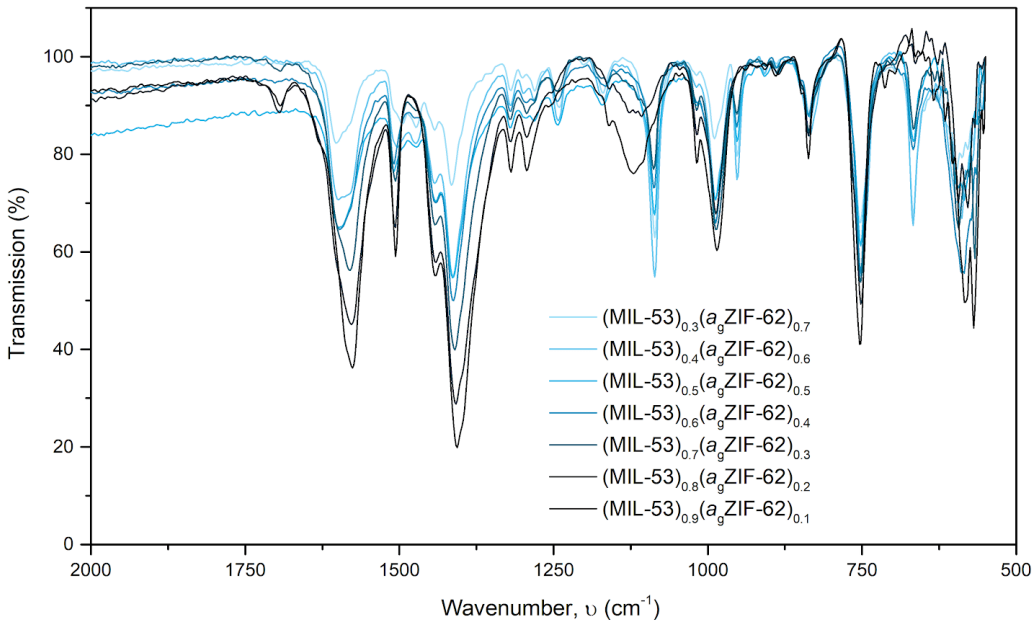

Supplementary Figure 33. Fourier transformed infra-red spectroscopy (FTIR) of $(MIL\text{-}53)_x(a_gZIF\text{-}62)_{1-x}$.

BET SURFACE AREA CALCULATIONS

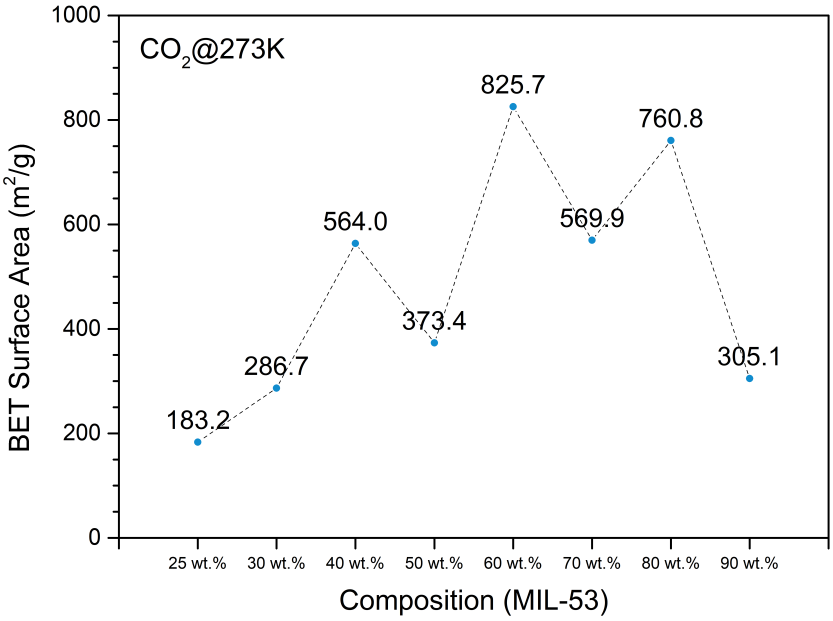

Supplementary Figure 34. BET surface areas of $(MIL\text{-}53)_x(a_gZIF\text{-}62)_{1-x}$ from CO_2 gas adsorption taken at 273 K.